RSC Advances

PAPER

View Article Online
View Journal | View Issue

Cite this: *RSC Adv.*, 2016, **6**, 93048

Exfoliation of graphite into graphene in aqueous solution: an application as graphene/TiO_2 nanocomposite to improve visible light photocatalytic activity

R. Giovannetti,*[a] E. Rommozzi,[a] M. Zannotti,[a] C. A. D'Amato,[a] S. Ferraro,[a] M. Cespi,[b] G. Bonacucina,[b] M. Minicucci[c] and A. Di Cicco[c]

Received 23rd March 2016
Accepted 23rd September 2016

DOI: 10.1039/c6ra07617c

www.rsc.org/advances

The aim of this study was the preparation of a graphene/TiO_2 heterogeneous catalyst supported on polypropylene for visible light photocatalysis. Aqueous graphene dispersions were prepared by liquid-phase exfoliation of graphite in the presence of a non-ionic surfactant, Triton X-100. The obtained graphene dispersion was characterized by X-ray diffraction, dynamic light scattering and UV-Visible spectroscopy and was subsequently used for the preparation of graphene/TiO_2 photocatalyst. As-prepared photocatalysts were tested for the photocatalytic degradation of a refractory dye, Alizarin Red S, in water solutions as target pollutant. Graphene/TiO_2 nanocomposites showed higher adsorption of Alizarin Red S on the catalyst surface and higher photocatalytic activity for its degradation under visible light irradiation, in respect to those obtained with pure TiO_2.

1. Introduction

Carbon is one of the most versatile elements in the periodic table in terms of the number of compounds that it may create; this is due to the types of bonds that it may form and to the number of different atoms that it can bond.[1]

The chemical nature of carbon in these materials comes from its hybridization states, which also determines the features of a variety of organic compounds.[2] Allotropes of carbon such as 0D fullerenes,[3] 1D carbon nanotubes[4] and 3D graphite and diamond[5,6] have been known for a long time.

The mother element of some carbon allotropes is graphene. Graphene is the 2D building block for all other dimensionalities of carbon materials. It can be wrapped up into 0D fullerenes, rolled into 1D nanotubes, or stacked into 3D graphite.[7]

The production of graphene in large quantities is an ongoing challenge for large-scale applications. Different processes are used to produce graphene from graphene oxide and need strong oxidizing and reducing agents. However, graphene fabricated under these chemical conditions tends to have a certain number of structural defects.[8] For that purpose, top-down methods such as the exfoliation of graphite powder in liquid-phase by sonication are a very promising routes due to their simplicity, versatility and low-cost;[9] besides, ultrasound treatment offers a suitable option to create high-quality graphene in great quantity.[8]

The direct exfoliation of graphite and a good dispersion of the resulting graphene sheets need to use stabilizers to prevent their stacking. Various stabilizers have been proposed, in both organic and aqueous media, such as ionic and non-ionic surfactants,[10] ionic liquids,[11] polymers,[12] organic salts[13] and aromatic molecules.[14]

Graphene with the thickness of a single carbon atom owns unique physical and chemical properties including highly flexible structure,[15] large surface area,[16] high electrical and thermal conductivity[17,18] and high chemical stability. Moreover, electrons in graphene have a linear relation between energy and momentum, so its band structure has no energy gap.[19] Accordingly, graphene is an attractive material in applications that require a fast electron transfer, such as energy storage[20,21] and photocatalysis.[22,23]

TiO_2 photocatalysis has emerged as a promising technology that could decisively contribute on the decrease of environmental pollution based on the utilization of solar energy. TiO_2 is mainly active under UV light irradiation due to its wide band gap (3.2 eV); considering that the percentage of UV light is less than 5% of the total solar spectrum incident on the earth, in recent years research has focused on the exploration of photocatalysts which would respond in the visible light region.[24]

Because of their properties, it has been reported that graphene based semiconductor nanocomposites are considered as good photocatalyst for pollutant degradation.[25] Graphene is an

[a]*School of Science and Technology, Chemistry Division, University of Camerino, Via S. Agostino 1, 62032 Camerino, Italy. E-mail: rita.giovannetti@unicam.it*

[b]*School of Pharmacy, University of Camerino, Via S. Agostino 1, 62032 Camerino, Italy*

[c]*School of Science and Technology, Physics Division, University of Camerino, Via Madonna delle Carceri 9, 62032 Camerino, Italy*

ideal nanomaterial for doping TiO_2 thanks to the formation of Ti–O–C bonds that extends the visible light absorption of TiO_2. Moreover, electrons are easily transported from TiO_2 to the graphene nano-sheets and the electron–hole recombination is significantly reduced, enhancing the oxidative reactivity.[26]

To test photocatalytic activity of new materials based on TiO_2, a high number of studies uses dyes as target pollutants.[23,27–30]

In our previous study we have successfully used polypropylene (PP) coated TiO_2 in the visible light photodegradation of Alizarin Red S (ARS) obtaining efficient dye degradation, with addition advantage of easy separation of photocatalyst and possibility of reuse.[31] ARS is a common water soluble anthraquinone dye extensively employed for cotton and silk dyeing and also used in clinical practices and in geology.[32] Due to synthetic origin and complex structure of aromatic rings, ARS is considered refractory pollutant difficult to remove by general chemical, physical and biological processes.[33] For this, wide ranges of technologies have been developed to remove this dye from wastewaters applying catalytic and photochemical methods.[34]

In this work, in order to obtain higher efficiently material, graphene/TiO_2 heterogeneous catalysts supported on polypropylene (PP) were prepared and investigated for the first time as visible light photocatalysts in water. To reach this aim, an aqueous solution of Triton X-100 has been used for the direct exfoliation of graphite by sonication to obtain graphene (GR) dispersion. Triton X-100 is a non-ionic surfactant able to work as dispersing agent and as stabilizer to prevent layer stacking. Graphene/TiO_2 heterogeneous catalysts supported on polypropylene (PP@GR–TiO_2) were prepared from the GR dispersion. PP@GR–TiO_2 nanocomposites were used to treat water with ARS as target pollutant by photocatalytic reaction under visible light.

2. Experimental

2.1. Reagents and materials

Timcal Timrex SFG44 Special Graphite (particle size: 5–75 μm) was purchased from Imerys Graphite & Carbon. Triton X-100 was supplied by Merck. Titanium(IV) dioxide anatase nanopowdered (code 718467, size <25 nm), Alizarin Red S, hydrochloric acid volumetric standard 1.0 N and acetyl acetone was bought from Sigma Aldrich. All of chemicals used were of analytical grade. Polycarbonate filter (25 mm, 0.2 μm) was a Whatman Nuclepore Track-Etched membrane (WHA110606). Catalyst support is constituted by polypropylene 2500 material obtained from 3 M. Deionized water was freshly prepared by a laboratory deionizer (Osmo Lab UPW 2).

2.2. Preparation of graphene dispersions

A series of GR dispersions were prepared by exfoliation of graphite in aqueous solution of 4% v/v Triton X-100 with ultrasonic cleaner Soltec Sonica 1200M (50 Hz to 80 W) and ultrasonic probe Hielscher UP100H (30 kHz to 100 W). Experimental conditions were reported in Table 1.

After ultrasonic treatments, dispersions were first centrifuged with a centrifuge Hermlez 323 K for 30 min at 3150 rpm and then for 30 min at 5150 rpm to sediment non-exfoliate graphite and to collect the GR dispersion. To obtain concentration data, a precisely measured volume of dispersion was filtered under high vacuum onto a polycarbonate membrane of known mass. The resulting film was washed with 25 mL of water, dried at room temperature and the mass was then determined using a microbalance.

2.3. Graphene characterization

GR dispersion was filtered under high vacuum onto a polycarbonate membrane for X-ray diffraction (XRD) measurements. XRD measurements were performed on a Debye–Scherrer diffractometer with an INEL CPS 180 position sensitive detector that allow to reduce drastically the acquisition time for each pattern. As X-ray source was used a Mo Kα radiation (λ = 0.7093 Å), generated by a Philips sealed X-ray tube and monochromatized through a graphite crystal along the 002 plane.

Different samples were prepared by H_2O dilution and by addition of various amounts of Triton X-100 to obtain the same surfactant concentrations and analysed by Dynamic Light Scattering (DLS) and UV-Visible (UV-Vis). DLS analysis was performed using Malvern Zetasizer nano S (Malvern instrument Worcestershire, UK) equipped with a back-scattered light detector operating at 173°. UV-Vis characterization was carried out with a Cary 8454 Diode Array System spectrophotometer (Agilent Technologies Measurements).

2.4. Photocatalysts preparation

In order to obtain PP@GR–TiO_2 photocatalysts, different amounts of graphene dispersion (containing 0.03, 0.06, 0.12 and 0.18 mg of GR) were added to TiO_2 during paste preparation by using TiO_2 anatase diluted with water, acetyl acetone and Triton X-100 as previously described.[31]

Successively, photocatalysts were supported on PP strips through dip coating technique, dried and clean with diluted HCl to remove the excess of TiO_2 particles.

2.5. Dye adsorption and photodegradation tests

ARS adsorption and photodegradation were investigated at 25 °C and at acidic pH by using a thermostated photo reactor. Initially, nine PP@mgGR–TiO_2 strips were immersed into solutions of ARS at concentrations ranging from 2.92×10^{-5} to 8.77×10^{-5} mol L^{-1}. Adsorption phase was performed for 2 h in dark conditions and successively, the system was exposed to

Table 1 Experimental conditions used for graphite exfoliation

Number test	Graphite (g)	Solvent (mL)	Ultrasonic bath (h)	Ultrasonic probe (h)
1	0.5	50	4	1
2	0.2	100	5	—
3	0.2	100	9	—

visible light (tubular JD lamp, 80 W, 1375 Lumen) and the photodegradation step took place.

Adsorption and photodegradation processes were monitored by UV-Vis, in real-time mode every 7 minutes, using a quartz cuvette in continuous flux (Hellma Analytics, 178.710-QS, light path 10 mm) connected through a peristaltic pump Gilson miniplus 3 to the photo reactor.

3. Results and discussions

3.1. Characterization of graphene dispersion

Water is usually considered as the better solvent, but it is inappropriate to exfoliate graphite or to disperse graphene. Thus, the maximum amount of water should be determined to guarantee the maximum production of graphene in aqueous solution. Water solution of Triton X-100 surfactant as co-solvent was used, as suggested by two reasons; one is because it is present in the catalyst paste formulation and the other because this non-ionic surfactant was described as active water dispersant of GR.[10] Obtained dispersions of GR were characterized by a dark grey colour. Images of graphite (a) and GR (b) dispersions in H_2O/Triton X-100 as solvent are reported in Fig. 1.

In order to obtain a structural characterization of GR, the dispersion was filtered and XRD measurements were carried out. In Fig. 2 XRD patterns of SFG44 graphite, SFG44 exfoliated graphite and its smoothed pattern were reported. In this figure (pattern c) is visible a broad peak (002) related to the periodic lamellar structure of graphite, that suggests a strong reduction of the long-range periodicity associated with the *c*-axis of graphite. However, after the exfoliation treatment, the other peaks of SFG44 graphite decreased significantly or disappeared. This confirm the loss of crystallinity of graphite structure after the ultrasound treatment and a random packing of graphene sheets.

In order to identify the best condition for the preparation of GR dispersions, DLS analysis was performed. In Fig. 3 are reported DLS spectra of GR dispersions obtained as a function of different preparation conditions (Table 1), with different GR concentrations, from 3.00 to 30.00 mg L^{-1} as reported in map legend, and with the same surfactant concentrations in all samples. All traces show the presence of three peaks. The peak at about 10 nm is associated to Triton X-100, that centred at about 220 nm is associated to GR, while the peak at about 5.56 μm is associated to non-exfoliate graphite remained at the end of the exfoliation process.

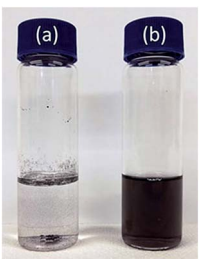

Fig. 1 Graphite (a) and GR (b) dispersions in H_2O/Triton X-100.

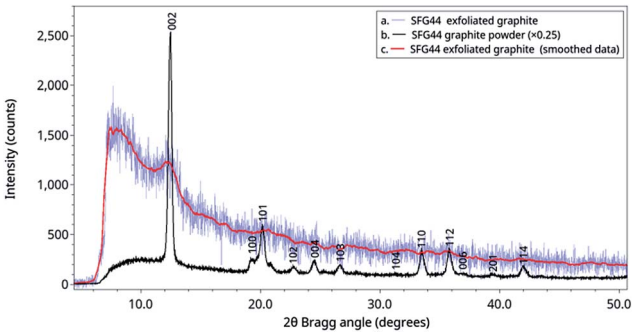

Fig. 2 XRD patterns of SFG44 exfoliated graphite by using an ultrasonic bath and collected on a filter (a, blue shaded line), SFG44 graphite powder (b, black line), and smoothed data of SFG44 exfoliated graphite (c, red line).

GR dispersion obtained by the test number 1 showed DLS spectra where the Triton X-100 and GR are characterized by peaks with different positions, width and, in same case, also shape; this is probably due to the high initial concentration of graphite and to the short ultrasonic time. GR dispersions obtained by test numbers 2 and 3 instead showed DLS spectra characterized by reproducible size distributions for Triton X-100 and GR. In addition, spectra of GR dispersions obtained by test number 2 were characterized by peaks of GR having a higher intensity compared to those obtained by the test number 3. This indicates that the condition applied in the test number 2 provided more concentrated GR dispersion in aqueous medium. For this reason, GR obtained at these conditions was further characterized and then applied in photocatalytic experiments. The GR concentration obtained by high vacuum filtration of a precisely measured volume of this dispersion was 30 mg L^{-1}.

Fig. 4 illustrates UV-Vis absorption spectra obtained by various dilutions with water up to 10 mL of as prepared exfoliated GR dispersion (in the map legend were reported dilution

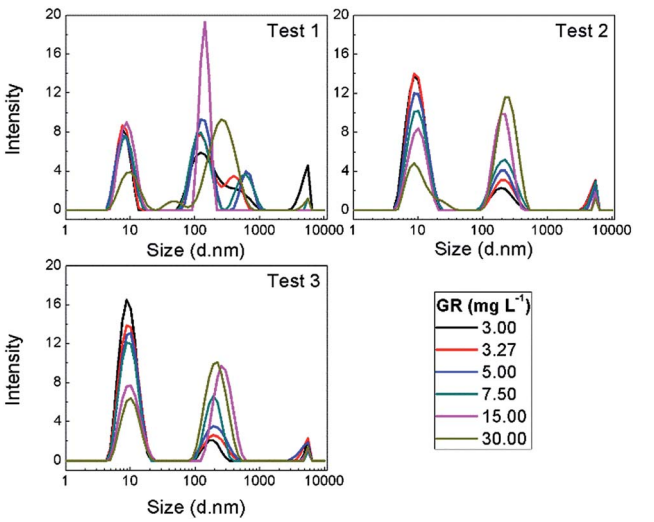

Fig. 3 DLS spectra of GR dispersions obtained by test number 1, 2 and 3 (Table 1) respectively; in the map legend GR concentrations in mg L^{-1} of all samples are reported.

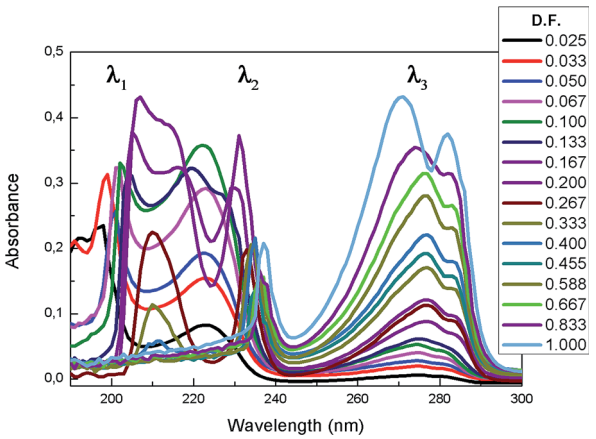

Fig. 4 UV-Vis absorption spectra of different amounts of GR dispersion obtained by dilution with water; in the map legend dilution factors (D.F.) of all samples are reported.

factors of all samples). Triton X-100 concentration varied from 1.284 to 0.032 g L^{-1} while GR concentration varied from 0.300 to 0.008 mg L^{-1}.

As it may be observed in the Fig. 4, spectra showed three different groups of bands in the region 190–290 nm (signed as λ_1, λ_2 and λ_3) with changes in wavelength and intensity for any specific Triton X-100 and GR concentration.

A detailed analysis of λ_2 showed a wavelength shift of the different dilutions of GR dispersion as function of Triton X-100 concentration (Fig. 5). In particular, a blue shift from 237 nm to 220 nm was firstly obtained when Triton X-100 concentration moved from 1.284 to 0.214 g L^{-1}, while a red shift from 220 nm to 223 nm was then observed at lower Triton X-100 concentration.

In the spectrum of Fig. 4 absorption bands at around 270 nm (λ_3), owing to π–π^* transitions of graphene,[35] for all dispersions were observed; the intensity of these bands depends by the GR amount and decreases according to the increase of dilution with water. It is possible to establish a linear Pearson relationship (adjusted determination coefficient = 0.99122) between the concentration of GR in H_2O/Triton X-100 solvent and the intensity of the corresponding absorbance spectrum at 270 nm as reported in Fig. 6.

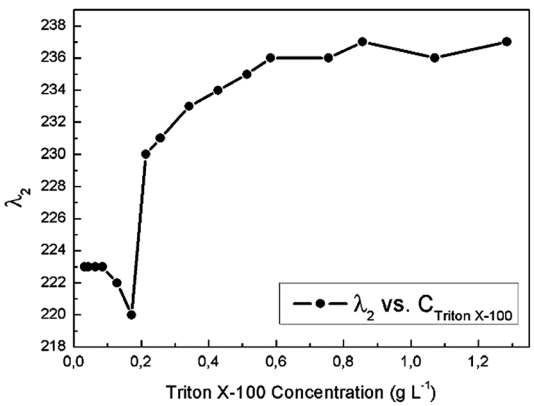

Fig. 5 λ_2 (nm) *versus* Triton X-100 concentration (g L^{-1}) after dilution.

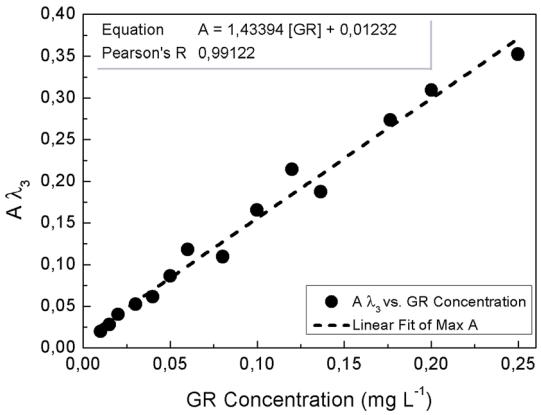

Fig. 6 Pearson correlation between GR concentration (mg L^{-1}) and the intensity of the corresponding absorbance at 270 nm.

To better understand the observed behaviour, the GR amount was keep constant varying only the Triton X-100 concentration. Fig. 7 illustrates UV-Vis absorption spectra obtained by dispersion of 0.008 mg of as prepared exfoliated GR with different amounts of Triton X-100 (in the map legend were reported the Triton X-100 concentration in g L^{-1} of all samples). In this case, the obtained spectra showed that, although the amount of GR is the same, the intensity of absorption band at around 270 nm increases with the increase of amount of Triton X-100. In addition, changes in wavelength and intensity were observed in the bands at around 190 and 240 nm at specific Triton X-100 concentrations.

A detailed analysis of λ_2 showed the change of wavelength as function of Triton X-100 concentration as reported in Fig. 8. A red shift from 224 nm to 236 nm was obtained with the increase of Triton X-100 concentration. This spectral change can be probably due to different interaction of Triton X-100 on exfoliated GR planes.

From the analysis of wavelength shifts, it is possible to deduce that the increase of surfactant concentration gives a red shift, while a blue shift is observed by increasing water. This

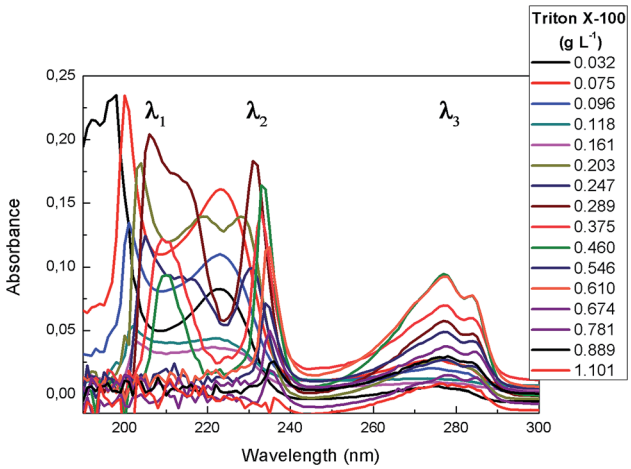

Fig. 7 UV-Vis absorption spectra obtained by 0.008 mg of GR with different amounts of Triton X-100; in the map legend Triton X-100 concentration in g L^{-1} of all samples are reported.

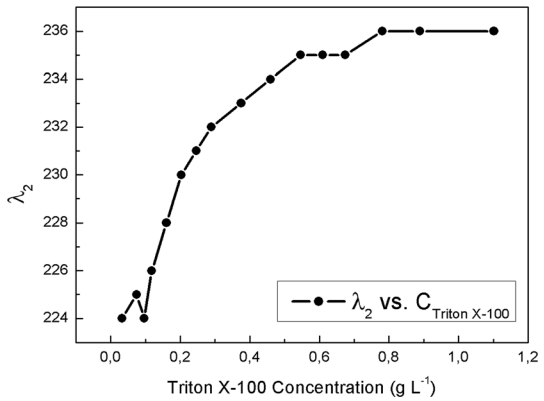

Fig. 8 λ_2 shift of GR dispersion as a function of Triton X-100 concentration (g L^{-1}).

behaviour is probably due to the variation of aggregation degree of graphene layers, depending to solvent composition. In particular, surfactant molecules balance the inter-sheet attractive forces of graphene flakes.

To confirm this hypothesis, DLS analysis was performed on samples prepared by various H_2O dilutions in which GR concentration varies from 3.0 to 30.0 mg L^{-1} while Triton X-100 concentration varies from 0.128 to 1.284 g L^{-1}.

Obtained spectra are reported in Fig. 9a. Analysing the central peak, it is possible to note a rightward shift (towards greater sizes) when the amount of water increases. Plotting the size change *versus* surfactant concentration (Fig. 9b), it is clearly visible a GR size increase although the total amount of GR decreases with the dilution. This behaviour can be explained considering that to a minor size correspond a higher Triton X-100 concentration.

DLS was also performed on GR dispersion with a GR concentration from 3.0 to 30.0 mg L^{-1} at constant Triton X-100 concentration (Fig. 10a). The different % of the intensity of both Triton X-100 and GR peaks is associated to the different amount

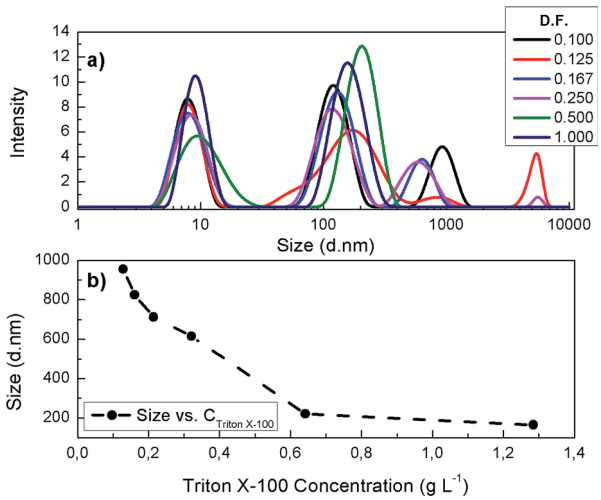

Fig. 9 DLS spectra of samples prepared by various H_2O dilutions (a); size (nm) *versus* Triton X-100 concentration (g L^{-1}) (b). In the map legend dilution factors (D.F.) of all samples are reported.

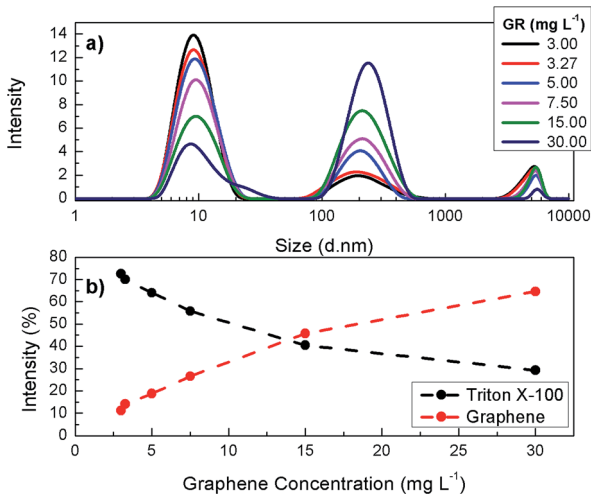

Fig. 10 Effect of GR concentrations (mg L^{-1}) on DLS spectra (a); intensity% of both GR and Triton X-100 *versus* GR concentration (mg L^{-1}) (b).

of GR in samples. In fact, at an increase of GR concentration corresponds an increase in intensity of the peak at 220 nm (associated with GR) without any variation of size, and a simultaneous decrease of the peak at 10 nm (associated with Triton X-100). This effect is shown in Fig. 10b.

Obtained results show that the exfoliated GR sheets have a size in the range 164–255 nm as a function of the Triton X-100 amount. Specifically, higher concentration of surfactant is necessary to reduce the graphene layers aggregation.

3.2. Dye adsorption on PP@mgGR–TiO_2 and photocatalytic application

GR dispersion was used for the preparation of PP@mgGR–TiO_2 catalysts.

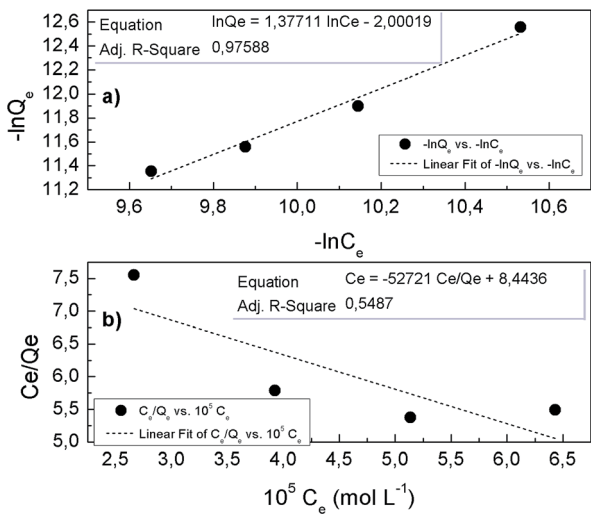

Fig. 11 Linear regression analysis of data using the Freundlich (a) and Langmuir (b) isotherms models.

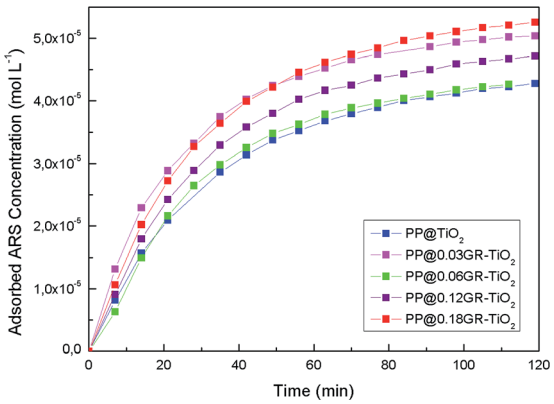

Fig. 12 Adsorbed concentration of ARS during time on different PP@mgGR–TiO_2 supports.

In the first step, in order to obtain information about dye adsorption process and equilibrium data, different starting ARS concentrations were used. The resulting absorbance changes were monitored at 424 nm for different ARS concentrations and analysed by linear forms of Freundlich (1) and Langmuir (2) isotherms models.[31]

$$Q_e = k_F C_e^{1/n} \quad (1)$$

$$Q_e = \frac{k_L C_e}{1 + a_L C_e} \quad (2)$$

In these equations, C_e is the ARS concentration in solution, Q_e is the concentration of ARS adsorbed on PP@mgGR–TiO_2 at the equilibrium, k_F is a constant value that represents the ability of adsorption, and $1/n$ is the adsorption intensity; k_L and a_L are the Langmuir constants.

The relationship of adsorption data of PP@mgGR–TiO_2 with Freundlich and Langmuir isotherms are reported in Fig. 11. The experimental data fit well with the Freundlich isotherm model (adjusted $R^2 = 0.976$) generating a k_F of 2.00 and $1/n$ of 1.38, confirming that, in the adsorption process of ARS on PP@mgGR–TiO_2, multilayer adsorption mechanism can occur as in the case of only TiO_2.[31]

The adsorbed concentration change of ARS on different PP@mgGR–TiO_2, is reported in Fig. 12 as function of time.

The analysed results followed a pseudo first order kinetic as expressed by eqn (3):[31]

Table 2 k_{ads} and k_{photo} with various catalysts

Catalyst name mgGR@TiO_2	$k_{ads} \times 10^2$ (min^{-1})	Adj. R_{ads}^2	$k_{photo} \times 10^3$ (min^{-1})	Adj. R_{photo}^2
PP@TiO_2	2.54	0.9967	7.70	0.9960
PP@0.03GR–TiO_2	3.28	0.9981	9.70	0.9949
PP@0.06GR–TiO_2	3.31	0.9966	11.5	0.9920
PP@0.12GR–TiO_2	3.30	0.9986	11.2	0.9924
PP@0.18GR–TiO_2	3.31	0.9996	12.5	0.9939

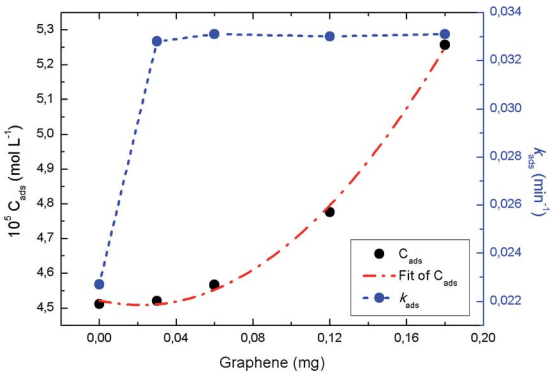

Fig. 13 C_{ads} and k_{ads} *versus* mg of GR.

$$\ln \frac{Q_e - Q_t}{Q_e} = -k_{ads} t \quad (3)$$

where Q_t is the amount of adsorbed ARS at time t, Q_e is the equilibrium concentration and k_{ads} is the pseudo first order adsorption rate constant. The plot of the first term of eqn (3) *versus* time for the different PP@mgGR–TiO_2 catalysts, provide k_{ads} and adjusted R^2 values reported in Table 2.

Trends of the absorbed ARS concentration (C_{ads}) at the end of adsorption process and k_{ads} *versus* mg of GR were reported in Fig. 13. All results showed that the presence of GR in TiO_2 influenced positively the absorption kinetics of ARS respect to pure TiO_2 but, in the range from 0.03 to 0.18 mg of GR, k_{ads} values were similar for all catalysts. On the contrary, with the increases of GR, in PP@mgGR–TiO_2, an increase of C_{ads} were observed for the concomitant GR adsorption due to π–π interactions and to increasing of absorption surface area. These nanocomposites showed higher adsorption performance of ARS respect to pure TiO_2 and the relationship between C_{ads} and the amount of graphene into catalysts can be described as a second order polynomial equation $C_{ads} = 3 \times 10^{-7}$ mgGR^2 to 4×10^{-7} mgGR + 5×10^{-5} with an adjusted determination coefficient of 0.998.

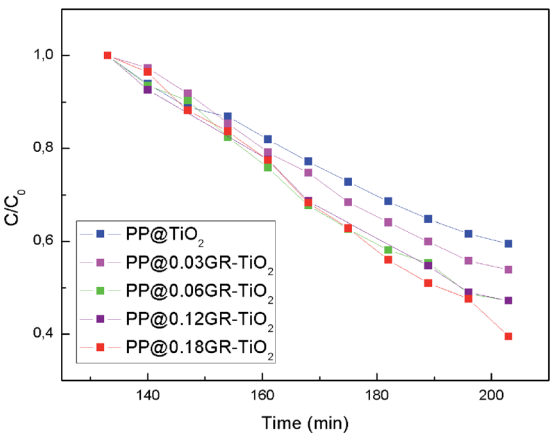

Fig. 14 Photodegradation of ARS as function of time with different PP@mgGR–TiO_2 as photocatalysts.

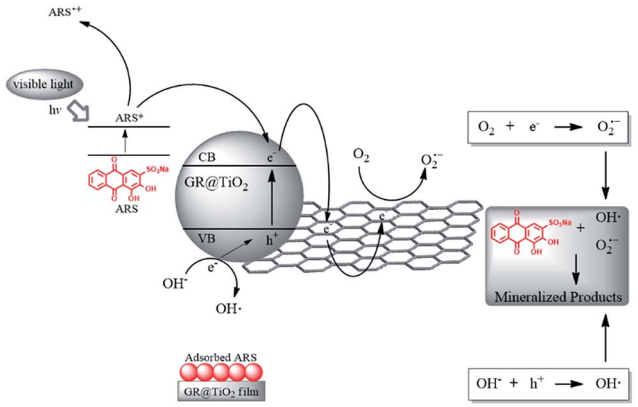

Fig. 15 Schematic representation of graphene/TiO_2 photocatalysis.

After ARS adsorption in dark conditions, in the second step, PP@mgGR–TiO_2 catalysts were utilized for photocatalytic degradation of ARS as a model reaction under visible-light. In Fig. 14 are reported the photodegradation of ARS during time for different PP@mgGR–TiO_2 photocatalysts, showing the positive effects of the presence of GR.

Kinetic evaluation of the photodegradation process of ARS showed that all as prepared PP@mgGR–TiO_2 catalysts follows first order model according to the eqn (4)[31]

$$\ln\frac{C}{C_0} = -k_{\text{photo}}t \quad (4)$$

where k_{photo} is related rate constants, C_0 is the initial concentration of ARS and C is the concentration of ARS at time t.

The plot of the first term of eqn (4) *versus* photodegradation time gives k_{photo} and adjusted R^2 values reported in Table 2. All results showed that, also in the photodegradation process, the presence of GR in TiO_2 influences positively photodegradation kinetics respect to pure PP@TiO_2 as demonstrated by the increase of k_{photo} values. While k_{ads} values were similar for all catalysts, the enhance of photocatalytic performance can be attributed of productive interaction between GR nano-sheets and TiO_2 in which the photogenerated electrons of TiO_2 are transferred on GR that act as electron acceptor inhibiting the electron–hole recombination.[36]

Obtained results prove that the addition of GR dispersion in the formulation of TiO_2 paste promote, thanks to the favourable interaction with Triton X-100, the homogeneity of GR and TiO_2 with consequent positive effect in efficacy of PP@GR–TiO_2 photocatalyst. By modulation of GR concentration in the paste formulation is therefore possible to increase the ARS absorption and the rate of photodegradation.

By previous study, by using PP@TiO_2,[31] photodegradation constant values were inversely proportional to the initial ARS concentration, showing that the increase of adsorbed dye on the photocatalyst decelerates the rate of the process. In this case, although the adsorbed ARS concentration increases on the PP@GR–TiO_2 due to positive effect of graphene, the obtained k_{photo} values showed the improvement of performance of this new photocatalyst.

A schematic representation of the mechanism of graphene/TiO_2 photocatalysis for ARS degradation is reported in Fig. 15.

4. Conclusions

Graphene dispersions were prepared using a simple and efficient exfoliation of graphite by liquid-phase sonication using an aqueous solution of Triton X-100 as co-solvent. The best preparation conditions were evaluated using XRD, DLS and UV-Vis analysis. The obtained GR dispersion was used to prepare graphene/TiO_2 nanocomposite that was for the first time supported on polypropylene. The obtained PP@mgGR–TiO_2 strips were used as photocatalytic materials for the ARS degradation in water solutions.

The presence of different amounts of GR showed positive effects increasing the adsorption of ARS on the catalyst surface, together with higher photocatalytic activity for dye degradation under visible light irradiation, respect to those obtained with pure PP@TiO_2.

Acknowledgements

We gratefully acknowledge financial support from the FAR Project 2015–2017 of Camerino University.

References

1 S. Ravi and S. Vadukumpully, *J. Environ. Chem. Eng.*, 2016, **4**, 835–856.
2 T. Kuila, S. Bose, A. K. Mishra, P. Khanra, N. H. Kim and J. H. Lee, *Prog. Mater. Sci.*, 2012, **57**, 1061–1105.
3 H. W. Kroto, J. R. Heath, S. C. O'Brien, R. F. Curl and R. E. Smalley, *Nature*, 1985, **318**, 162–163.
4 S. Iijima, *Nature*, 1991, **354**, 56–58.
5 Y. Hernandez, S. Pang, X. Feng and K. Müllen, *Polymer Science: A Comprehensive Reference*, 2012, vol. 8, pp. 415–438.
6 C. Frondel and U. B. Marvin, *Nature*, 1967, **214**, 587–589.
7 A. K. Geim and K. S. Novoselov, *Nat. Mater.*, 2007, **6**, 183–191.
8 A. M. Dimiev and J. M. Tour, *ACS Nano*, 2014, **8**, 3060–3068.
9 A. Ciesielski and P. Samorì, *Chem. Soc. Rev.*, 2014, **43**, 381–398.
10 L. Guardia, M. J. Fernàndez-Merino, J. I. Paredes, P. Solìs-Fernàndez, S. Villar-Rodil, A. Martìnez-Alonso and J. M. D. Tascòn, *Carbon*, 2011, **49**, 1653–1662.
11 A. T. Najafabadi and E. Gyenge, *Carbon*, 2014, **71**, 58–69.
12 Z. Sun, S. Poller, X. Huang, D. Guschin, C. Taetz, P. Ebbinghaus, J. Masa, A. Erbe, A. Kilzer, W. Schuhmann and M. Muhler, *Carbon*, 2013, **64**, 288–294.
13 W. Du, J. Lu, P. Sun, Y. Zhu and X. Jiang, *Chem. Phys. Lett.*, 2013, **568–569**, 198–201.
14 X. Dong, Y. Shi, Y. Zhao, D. Chen, J. Ye, Y. Yao, F. Gao, Z. Ni, T. Yu, Z. Shen, Y. Huang, P. Chen and L. J. Li, *Phys. Rev. Lett.*, 2009, **102**, 135501.
15 C. Lee, X. Wei, J. W. Kysar and J. Hone, *Science*, 2008, **321**, 385–388.
16 M. D. Stoller, S. Park, Y. Zhu, J. An and R. S. Ruoff, *Nano Lett.*, 2008, **8**, 3498–3502.

17 K. S. Novoselov, A. K. Geim, S. V. Morozov, D. Jiang, Y. Zhang, S. V. Dubonos, I. V. Grigorieva and A. A. Firsov, *Science*, 2004, **306**, 666–669.
18 A. A. Balandin, S. Ghosh, W. Bao, I. Calizo, D. Teweldebrhan, F. Miao and C. N. Lau, *Nano Lett.*, 2008, **8**, 902–907.
19 T. N. Arama and A. Asgari, *Phys. Lett. A*, 2015, **379**, 974–978.
20 N. Li, G. Liu, C. Zhen, F. Li, L. Zhang and H. M. Cheng, *Adv. Funct. Mater.*, 2011, **21**, 1717–1722.
21 F. Maroni, R. Raccichini, A. Birrozzi, G. Carbonari, R. Tossici, F. Croce, R. Marassi and F. Nobili, *J. Power Sources*, 2014, **269**, 873–882.
22 A. Ajmal, I. Majeed, R. N. Malik, H. Idriss and M. A. Nadeem, *RSC Adv.*, 2014, **4**, 37003–37026.
23 D. Zhao, G. Sheng, C. Chen and X. Wang, *Appl. Catal., B*, 2012, **111–112**, 303–308.
24 Y. Gua, M. Xinga and J. Zhang, *Appl. Surf. Sci.*, 2014, **319**, 8–15.
25 N. R. Khalid, E. Ahmed, Z. Hong, L. Sana and M. Ahmed, *Curr. Appl. Phys.*, 2013, **13**, 659–663.
26 H. Zhang, X. Lv, Y. Li, Y. Wang and J. Li, *ACS Nano*, 2010, **4**, 380–386.
27 Z. Zhao, Y. Wang, J. Xu and Y. Wang, *RSC Adv.*, 2015, **5**, 59297.
28 Z. Xiong, L. L. Zhang, J. Ma and X. S. Zhao, *Chem. Commun.*, 2010, **46**, 6099–6101.
29 Y. Wen, H. Ding and Y. Shan, *Nanoscale*, 2011, **3**, 4411–4417.
30 C. Chen, W. Cai, M. Long, B. Zhou, Y. Wu, D. Wu and Y. Feng, *ACS Nano*, 2010, **4**, 6425–6432.
31 R. Giovannetti, C. A. D'Amato, M. Zannotti, E. Rommozzi, R. Gunnella, M. Minicucci and A. Di Cicco, *Sci. Rep.*, 2015, **5**, 17801.
32 J. A. D. Dickson, *J. Sediment. Petrol.*, 1966, **36**, 491–505.
33 R. K. Gautam, A. Mudhoo and M. C. Chattopadhyaya, *J. Environ. Chem. Eng.*, 2013, **1**, 1283–1291.
34 G. Palmisano, V. Augugliaro, M. Pagliaro and L. Palmisano, *Chem. Commun.*, 2007, **33**, 3425–3437.
35 Y. Zhang, S. Liu, L. Wang, X. Qin, J. Tian, W. Lu, G. Changa and X. Sun, *RSC Adv.*, 2012, **2**, 538–545.
36 X. Bai, X. Zhang, Z. Hua, W. Ma, Z. Dai, X. Huang and H. Gu, *J. Alloys Compd.*, 2014, **599**, 10–18.